Available online at www.sciencedirect.com
ScienceDirect
Journal of Power Sources 174 (2007) 282–293
JOURNAL OF POWER SOURCES
www.elsevier.com/locate/jpowsour

Experimental and numerical analysis of dynamic metal hydride hydrogen storage systems

Brendan D. MacDonald *, Andrew M. Rowe

Institute for Integrated Energy Systems, Department of Mechanical Engineering, University of Victoria, P.O. Box 3055 STN CSC, Victoria, B.C. V8W 3P6, Canada

Received 28 August 2007; accepted 10 September 2007
Available online 14 September 2007

Abstract

This paper examines the dynamics of metal hydride storage systems by experimentation and numerical modelling. A specially designed and instrumented metal hydride tank is used to gather data for a cyclic external hydrogen load. Thermocouples provide temperature measurements at various radial and axial locations in the metal hydride bed. This data is used to validate a two-dimensional mathematical model previously developed by the authors. The model is then used to perform a parametric study on some of the key variables describing metal hydride systems. These variables are the equilibrium pressure, where the tails and concentration dependence are investigated, and the effective thermal conductivity of the metal hydride bed, where the pressure and concentration dependence are analyzed. Including tails on the equilibrium pressure curves was found to be important particularly for the accuracy of the initial cycles. Introducing a concentration dependence for the plateau region of the equilibrium pressure curve was found to be important for both pressure and temperature results. Effective thermal conductivity was found to be important, and the inclusion of pressure and concentration dependence produced more precise modelling results.

Keywords: Hydrogen storage; Metal hydride; Thermal conductivity; Heat transfer; Dynamic; Numerical model

1. Introduction

Hydrogen storage in reversible metal hydrides is attractive because it can be stored at relatively low pressures with a high volumetric density. Metal hydride systems are particularly advantageous for stationary or small-scale fuel cell applications, where the desire for small storage tanks outweighs the disadvantages of metal hydride mass.

A significant issue for metal hydride storage systems is limited heat transfer between the fluid on the exterior of the tank and the metal hydride alloy within the tank where the reaction is taking place. Often, heat transfer determines the rate at which hydrogen gas can be extracted from a tank [1]. Increasing heat transfer rates is important for optimizing the design of metal hydride hydrogen storage applications.

There have been a number of previous studies aimed at understanding and optimizing the behaviour of metal hydride vessels, particularly through the use of numerical models [2–20]. To accompany the numerical studies, there have been some experimental investigations performed. The experimental work has focused on validating numerical models directly [2,4,5,11,15], as well as determining key characteristics of metal hydride beds, such as effective thermal conductivity [21–27]. Numerous attempts to create empirical relationships describing effective thermal conductivity have resulted from some of the experimental work [21,22,25,28,29].

There has been relatively little work done pertaining to dynamic investigations for actual hydrogen storage system applications. One of the things that is missing from the scientific community are some in depth studies of how metal hydride storage systems behave in dynamic applications, where they will invariably face cycling in their usage patterns. Some past dynamic investigations [18,30] show that there are distinct advantages when metal hydride beds are thermally coupled to fuel cells in cyclical applications. This study aims to experimentally validate and further improve upon a numerical model that can be utilized to simulate dynamic scenarios for enhancing metal hydride systems.

* Corresponding author. Tel.: +1 250 7218920; fax: +1 250 7216051.
E-mail address: bdmacdon@hotmail.com (B.D. MacDonald).

0378-7753/$ – see front matter © 2007 Elsevier B.V. All rights reserved.
doi:10.1016/j.jpowsour.2007.09.021

Nomenclature

P	pressure (kPa)
P_{eq}	equilibrium pressure (kPa)
P_{eqa}	equilibrium pressure for absorption (kPa)
P_{eqd}	equilibrium pressure for desorption (kPa)
T	temperature (K)
Greek letters	
ρ_{emp}	density of the metal hydride at empty state ($kg\,m^{-3}$)
ρ_s	density of the metal hydride ($kg\,m^{-3}$)

This investigation begins with experimental work to determine the PCT behaviour, and thermal conductivity of a commercially available AB_2 type alloy, with properties similar to $Ti_{0.98}Zr_{0.02}V_{0.43}Fe_{0.09}Cr_{0.05}Mn_{1.5}$. Bernauer et al. [31] provide detailed information on the fundamentals and properties of this alloy, but there is relatively limited information available in the literature on the heat transfer characteristics. Once this data has been acquired the numerical model developed by the authors in a previous study [17] is validated by dynamic experiments. Dynamic desorption experiments using a mass flow controller are used to generate temperature and pressure time series corresponding to a simple harmonic load profile. This data is analyzed and compared to the results generated by using a two-dimensional transient model to simulate the same conditions as the experiment. Sensitivity studies are performed for the PCT curve and effective thermal conductivity to uncover which aspects have the biggest impact on model accuracy.

2. Tank design details

The metal hydride vessel used in this study is shown schematically in Fig. 1. The tank body was machined from a solid block of 6061-T6 aluminum and designed to hold 0.27 L of metal hydride powder, which equates to approximately 840 g of the alloy used in this study. The internal diameter of the tank is 5.8 cm, the height of the hydride bed is approximately 10.5 cm, and the thickness of the aluminum is 4 mm. The commercially available alloy used in this study has properties similar to $Ti_{0.98}Zr_{0.02}V_{0.43}Fe_{0.09}Cr_{0.05}Mn_{1.5}$. An anaerobic glove box is used to transfer the activated metal hydride powder between vessels to prevent poisoning and pyrophoric behaviour. The metal hydride bed is held in place by a series of Delrin spacers combined with fine nylon mesh and filter paper. The spacers at the top of the tank are designed to keep the alloy in place while still allowing hydrogen to flow through a pattern of holes. The spacers at the bottom of the tank are designed to hold the alloy in place while also keeping the thermocouples in position. Six thermocouples are arranged throughout the hydride bed as shown in Fig. 2 to allow for the measurement of temperature along the radial direction as well as along the tank height (axial symmetry is assumed). In Fig. 2 thermocouples 1–4 (labelled as TC 1–4) are reading at a height in the middle of the metal hydride bed, thermocouple 5 is reading at a height 2.54 cm above the mid-line, and thermocouple 6 is reading at a height 2.54 cm below the mid-line. As shown in the photograph of the assembled tank in Fig. 3, another thermocouple is attached to the exterior of the tank using metal foil tape to estimate the external wall temperature. The tank is sealed by flanges on the top and bottom which compress o-rings to ensure a proper seal. The top flange includes both a pressure relief and quick connect valve for safety and ease of use. The thermocouples are sealed and attached to the bottom flange using Swagelok fittings. The accuracy of the thermocouples used in this study is ±1.0 °C.

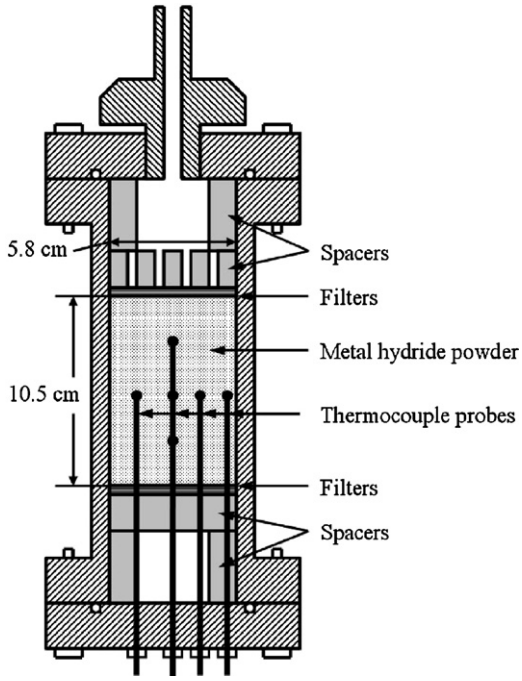

Fig. 1. Schematic of the instrumented metal hydride tank designed and fabricated for this study.

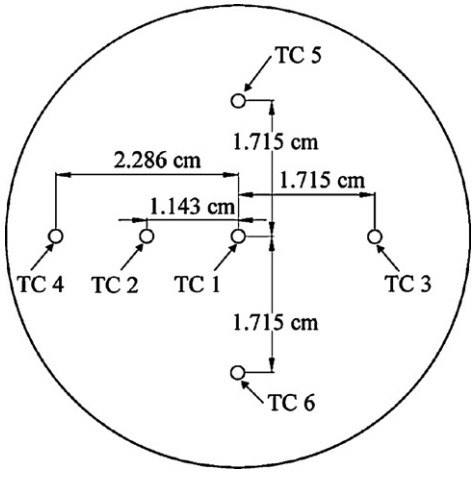

Fig. 2. Schematic of the interior of the metal hydride tank, showing the placement and distribution of thermocouples.

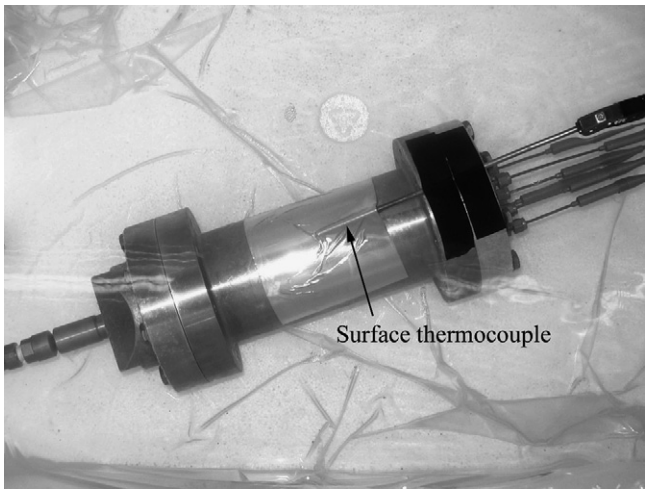

Fig. 3. Photograph of the assembled metal hydride tank.

3. Experimental apparatus

A schematic of the experimental apparatus used in this study is shown in Fig. 4. The metal hydride vessel is placed in a temperature controlled water bath connected to a Neslab RTE-740 refrigerated bath/circulator. Manual valves enable the system to perform hydrogen filling and emptying of the tank, operation with the hydrogen reservoir, and to switch between a vacuum pump and exhaust port for evacuation. The hydrogen filling portion of the system involves a high-pressure cylinder as the source of the hydrogen, a regulator to control the pressure, a Sierra mass flow controller to control the incoming flow of hydrogen, and a Hastings mass flow meter to provide additional measurement of the mass flow rate. The discharge portion of the system also has a mass flow controller and a mass flow meter for hydrogen flow control and measurement, and it has the option of flowing directly to the atmosphere or utilizing a vacuum pump to drain the metal hydride tank. The mass flow controllers are wired to the data acquisition system which allows the hydrogen flow to be controlled by Labview programming. Use of Labview enables dynamic simulations to be performed on the hydride vessel. The 1.83 L hydrogen reservoir can be filled and vacuumed separately from the metal hydride tank thus allowing for measured amounts of hydrogen to be added or extracted from the hydride vessel. This allows a PCT curve to be generated as described in Section 4. Two Omega pressure transducers enable pressure measurements to be taken for the incoming hydrogen gas source and inside of the metal hydride vessel as shown in Fig. 4. The accuracy of the pressure transducers is ±0.25% of full scale (±17 kPa for the incoming transducer and ±9 kPa for the metal hydride tank transducer).

4. Experimental determination of PCT curves

The PCT curve of the alloy was determined using the apparatus described in Section 3. The experimental procedure began by using a vacuum pump to create a low pressure in the tank (∼3 kPa) at a high temperature (∼50 °C) for an extended period of time (∼12 h) to ensure that the metal hydride bed began the experiment in an empty state. The canister was then brought to the temperature that would be used for the experiment by setting the chiller to maintain the temperature of the water bath (23 °C and 10 °C). A bottle of pure (99.999) hydrogen was used to fill the hydrogen reservoir to predetermined pressure levels. The metal hydride tank and hydrogen reservoir were then connected and allowed to reach an equilibrium state. The pressure and temperature of the metal hydride vessel and hydrogen reservoir were measured at the initial and final states. The hydrogen reservoir was filled again and the process repeated step by step until the metal hydride bed reached a pressure close to the maximum pressure of the regulator (∼1650 kPa absolute). This procedure yields an isothermal absorption curve. The metal hydride vessel was maintained at 23 °C for the first experiment. It can be seen from the results in Fig. 5 that the maximum pressure did not allow for the upper tail of the PCT curve to be shown at this temperature. The absorption test was repeated for a temperature of 10 °C. Fig. 5 shows that a small upper tail was recorded at this temperature indicating that the filling had covered the entire plateau region.

A desorption curve was created by beginning at the final point of the 10 °C absorption test. The hydrogen reservoir was vacuumed down using the vacuum pump and then connected to the metal hydride tank and allowed to reach an equilib-

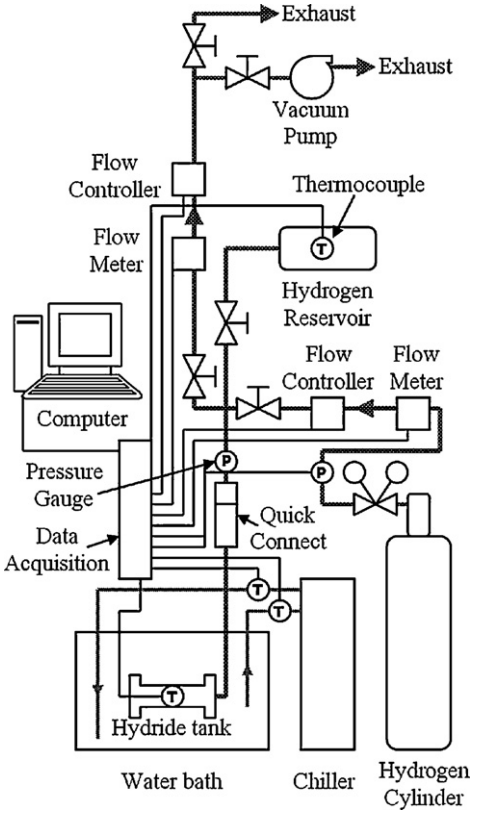

Fig. 4. Schematic of the experimental apparatus.

rium state. The hydrogen reservoir was then vacuumed down again and the process was repeated many times until the equilibrium pressure in the metal hydride tank was sufficiently close to the vacuum pressure. Because the volume, temperature, and pressure of the reservoir and metal hydride tank are known, the ideal gas law was used to determine the mass of hydrogen absorbed or desorbed by the metal hydride bed during each step.

Using the experimental results shown in Fig. 5, an equation describing the equilibrium pressure of the system can be generated. Based on the results from Bernauer et al. [31] and assuming negligible hysteresis, the van't Hoff equation for $Ti_{0.98}Zr_{0.02}V_{0.43}Fe_{0.09}Cr_{0.05}Mn_{1.5}$ is

$$\ln P_{eq} = 18.089 - \frac{3295.6}{T} \quad (1)$$

where P_{eq} and T are the equilibrium pressure (kPa absolute) and temperature (K) of the metal hydride bed, respectively. Based on a curve fit of the measured data in this study, at the middle of the plateau region (5548.5 kg m^{-3}), the van't Hoff expressions for absorption and desorption are

$$\ln P_{eqa} = 16.036 - \frac{2667.3}{T} \quad (2)$$

$$\ln P_{eqd} = 15.556 - \frac{2667.3}{T} \quad (3)$$

As seen from Fig. 5, the plateau region is not flat and the equilibrium pressure is a function of hydrogen concentration in the metal hydride. This has been noted in other alloys such as $LaNi_5$ [11], where a polynomial was created to describe the entire PCT curve as a function of concentration and temperature. In this work, an expression has been derived to describe the plateau region, with hydrogen concentration and temperature dependence. The modified van't Hoff expressions are as follows:

$$\ln P_{eqa} = 0.01116(\rho_s) - \frac{2667.3}{T} - 54.54 \quad (4)$$

$$\ln P_{eqd} = 0.01116(\rho_s) - \frac{2667.3}{T} - 55.02 \quad (5)$$

where ρ_s is the density of the metal hydride bed. It can be seen from the comparison in Fig. 5 that these expressions yield a plateau pressure that is similar to the experimental results. During the parametric analysis in Section 8.2 the effects of including the hydrogen concentration dependence will be examined.

Initial numerical simulations using only the plateau region of the PCT curve did not give results corresponding to experimental observations. It was determined that the tails of the PCT curve, particularly the upper tail, would give more accurate modelling results. The tail regions are identified and defined in Fig. 6. The importance of the tail regions is due to the way in which metal hydride tanks are generally filled and the conditions at which they are emptied. Typically, a tank is cooled and exposed to a high-pressure hydrogen source during filling, which can result in the system reaching a point somewhere into the upper tail region (illustrated in Fig. 6 as point A). Subsequently, when the tank is set up for discharge, for example when hooked up to a fuel cell or other energy converter, it may be heated by a separate heat source or the waste heat from the energy converter [18]. This results in a starting point that can be a significant distance into the upper tail region at this higher temperature due to the narrowing of the two-phase region as pressure increases (illustrated in Fig. 6 as point B).

To include the tail regions of the PCT curve in their model, Jemni et al. [11] used a ninth order polynomial to describe the entire PCT curve as noted above. To simplify curve fitting, the experimental PCT curve was approximated using three different sections, the lower tail, plateau, and upper tail. The natural logarithm of pressure is described by a second order

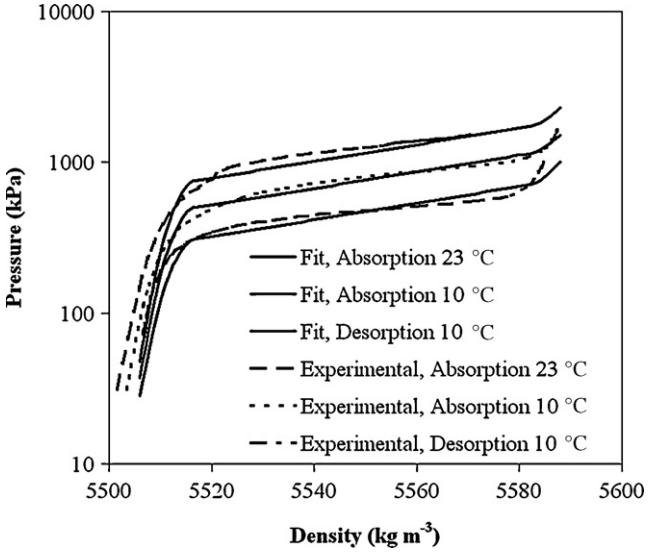

Fig. 5. Comparison of the equilibrium pressure curves that were experimentally determined and the theoretical curves used in the numerical model.

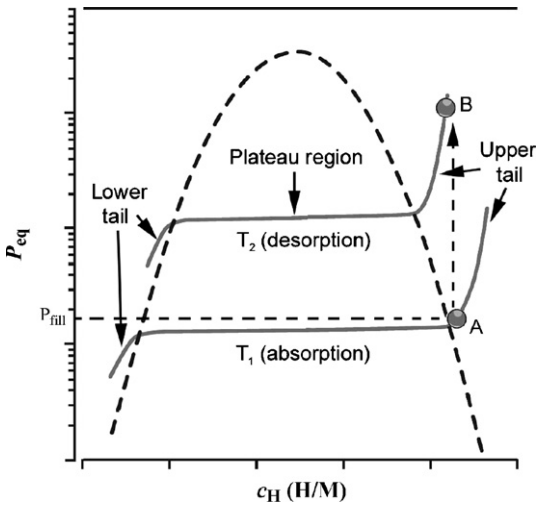

Fig. 6. Pressure–composition curve describing terminology and demonstrating what can happen during the filling and heating of a tank.

polynomial (for the tails) or a linear expression (for the plateau) with the three expressions creating a piece-wise continuous function. The modified equilibrium pressure expressions are as follows:

- Absorption

$$\text{for } (5517 \le \rho_s \le 5580),$$
$$\ln P_{eqa} = 0.01272(\rho_s) - \frac{2667.3}{T} - 54.54$$
$$\text{for } (\rho_s < 5517),$$
$$\ln P_{eqa} = \left(0.01272(5517) - \frac{2667.3}{T} - 54.54\right) \times \left[1 - \frac{(\rho_s - 5517)^2}{(\rho_{emp} - 5517)^2}\right] \quad (6)$$
$$\text{for } (\rho_s > 5580),$$
$$\ln P_{eqa} = 0.0048(\rho_s - 5580)^2 + \left(0.01272(5580) - \frac{2667.3}{T} - 54.54\right)$$

- Desorption

$$\text{for } (5517 \le \rho_s \le 5580),$$
$$\ln P_{eqd} = 0.01272(\rho_s) - \frac{2667.3}{T} - 55.02$$
$$\text{for } (\rho_s < 5517),$$
$$\ln P_{eqd} = \left(0.01272(5517) - \frac{2667.3}{T} - 55.02\right) \times \left[1 - \frac{(\rho_s - 5517)^2}{(\rho_{emp} - 5517)^2}\right] \quad (7)$$
$$\text{for } (\rho_s > 5580),$$
$$\ln P_{eqd} = 0.0059(\rho_s - 5580)^2 + \left(0.01272(5580) - \frac{2667.3}{T} - 55.02\right)$$

where ρ_{emp} is the density of the metal hydride bed at empty state. The impact of using an equilibrium pressure with and without tails is examined in Section 8.1.

5. Experimental and numerical thermal conductivity analysis

Thermal conductivity data for an "empty" tank was collected using the test apparatus. The tank was evacuated using the vacuum pump to ensure that no heat of reaction would exist. Once the bed had reached a hydrogen pressure of ~5 kPa the temperature was changed to each of the following values and held for 12 h: 60 °C, 30 °C, 50 °C, and 20 °C. During this process the temperatures in the bed were recorded. This data was then plotted and compared to results generated by the numerical model while altering the thermal conductivity. Values of thermal conductivity were varied until the predicted temperature responses were similar to the experimental data. The value of thermal conductivity yielding a reasonable match is

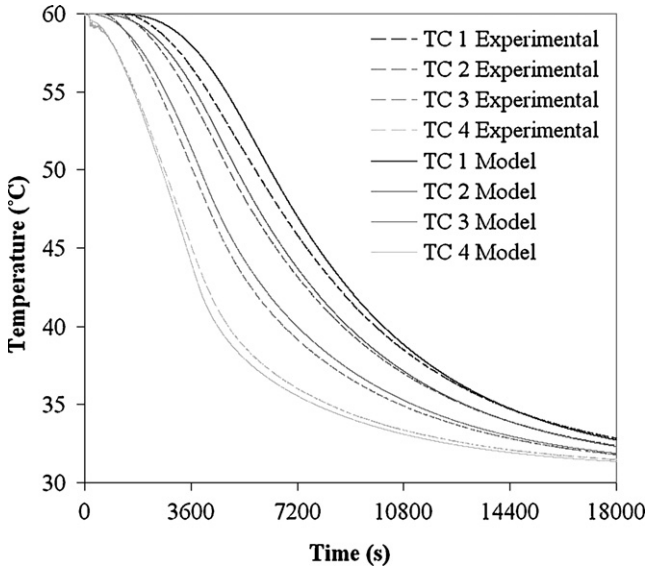

Fig. 7. Comparison of the experimental and theoretical temperature for one step in the process of determining the thermal conductivity value, from 60 °C to 30 °C.

0.045 W m K^{-1}. Fig. 7 shows the experimental data compared to the numerical data for the first temperature step (60–30 °C). The maximum temperature difference between any single probe and the predicted value differs by less than 2 °C over the entire transient.

A review of past literature for thermal conductivity of metal hydride beds [21–29], uncovered minimal variation between most of the effective thermal conductivity expressions, in the pressure ranges encountered in this study. For this work the thermal conductivity is described by an expression that is similar to one developed in a previous paper [21]:

$$k_e = 0.56 + 0.19\ln\left(\frac{P}{1000}\right) + 0.006\left(\ln\left(\frac{P}{1000}\right)\right)^2 - 0.0052\left(\ln\left(\frac{P}{1000}\right)\right)^3 + 0.46\left(\frac{H}{M}\right) \quad (8)$$

where k_e, P, and H/M are the effective thermal conductivity (W m^{-1} K^{-1}), absolute pressure (kPa) of the metal hydride bed, and the hydrogen-to-metal atomic ratio. This expression was derived empirically for $TiMn_{1.5}$ hydride. Eq. (8) was altered to match more closely with the experimentally determined thermal conductivity value at low pressures and for a closer match to the dynamic experimental observations to yield the following expression for the effective thermal conductivity of the metal hydride in this study:

$$k_e = 0.57 + 0.361\ln\left(\frac{P}{100}\right) + 0.0114\left(\ln\left(\frac{P}{100}\right)\right)^2 - 0.00988\left(\ln\left(\frac{P}{100}\right)\right)^3 + 48.12\left(\frac{\rho_s - \rho_{emp}}{\rho_{emp}}\right) \quad (9)$$

In Section 8.3, the impact of using a constant thermal conductivity value versus Eq. (9) is investigated.

Table 1
Properties of the tank wall material, aluminum 6061-T6 [32]

Parameter	Value
Density, ρ (kg m^{-3})	2770
Specific heat, c_p (J kg^{-1} K^{-1})	875
Thermal conductivity, k (W m^{-1} K^{-1})	177

Table 2
Properties of the metal hydride alloy, $Ti_{0.98}Zr_{0.02}V_{0.43}Fe_{0.09}Cr_{0.05}Mn_{1.5}$

Parameter	Value
Saturated density, ρ_{sat} (kg m^{-3})	5595
Empty density, ρ_{emp} (kg m^{-3})	5500
Specific heat, c_p (J kg^{-1} K^{-1})	490
Permeability, K (m^2) [assumed]	10^{-8}
Reaction heat of formation, ΔH° (J kg^{-1})	-1.10×10^7
Porosity, ε	0.4301

6. Metal hydride model

The model used to describe the behaviour of the metal hydride was derived and utilized by the authors in two previous papers [17,18]. In this study there are two subdomains, one representing the metal hydride alloy and another representing the aluminum tank walls. The walls are assumed to be 6061-T6 aluminum (properties are summarized in Table 1). They are shown in Fig. 8 as the unshaded region around the exterior of the metal hydride alloy subdomain, which is the shaded region. The dimensions of the subdomains match the experimental case described above with an outer tank radius of 3.3 cm, a height of 10.5 cm, and aluminum wall thickness of 4 mm.

The key metal hydride properties are summarized in Table 2. The PCT behaviour is described by Eqs. (6) and (7). Hysteresis is included in the model by utilizing two distinct equations for the absorption and desorption pressures. The effective thermal conductivity of the metal hydride bed is described by Eq. (9). The model also assumes thermal equilibrium between the hydrogen and metal hydride alloy at any location within the tank.

7. Dynamic model validation and fitting

7.1. Experimental work

Much of the previous validation work for numerical metal hydride models has been performed under steady flow conditions, whereby a tank is usually emptied or filled in one smooth step. Here, the model will be validated using dynamic data during a cyclic desorption event. Utilizing the experimental apparatus described in Section 3 and the instrumented metal hydride tank in Section 2 a sinusoidal load was experimentally created. For these experiments the temperature was fixed in the water bath by the chiller. Three sets of experiments were performed at a temperature of 25 °C, and two sets were performed at 35 °C. Labview was used to set the mass flow controller to create sinusoidal hydrogen mass flows as shown in Fig. 9a and b.

After the tank was filled at a temperature of 10 °C to a hydrogen pressure of ∼1650 kPa (absolute), it was allowed to reach equilibrium at the desired temperature of the experiment. At this point software control was initiated and the flow controller began to allow hydrogen to exit the tank at the programmed levels. The flow controller is able to create sinusoidal flow until there is insufficient pressure in the tank to do so (∼650 kPa absolute), at which point the controller is unable to control the flow and the experiment is terminated. The actual hydrogen flow recorded by the flow controller is shown in Fig. 9a and b for the 25 °C and 35 °C cases, respectively along with the flow pattern that was entered in the numerical model as a top surface boundary condition, and the command flow sent to the controller. The temperature readings for thermocouples 3, 5, and 6 were found to be equivalent within the accuracy range of the thermocouples for the dynamic experimentation. Because of this low variation, the study focuses on radial temperature differences and not height variances.

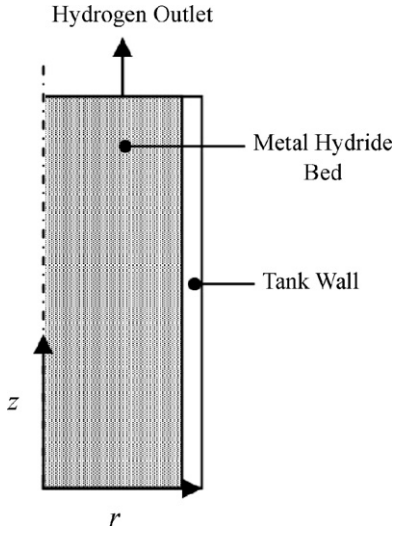

Fig. 8. Schematic of metal hydride tank used in numerical model.

7.2. Validation of model

The numerical model was used to simulate the same conditions experienced in the experimental work and the results are compared to the experimental pressures and temperatures. Fig. 10a and b compares the measured tank pressure with the modelled prediction for bath temperatures of 25 °C and 35 °C. Fig. 11a and b compares the measured and predicted temperatures. The temperature curves predicted by the model show higher variation for each cycle and there is a greater spread of temperatures along the radial direction as cycling progresses. Correcting for this minor variation from the experimental results by increasing the effective thermal conductivity would also cause a change in the pressure curves of Fig. 10a and b. A compromise was made to allow for the closest match between pressures and temperatures. The adjust-

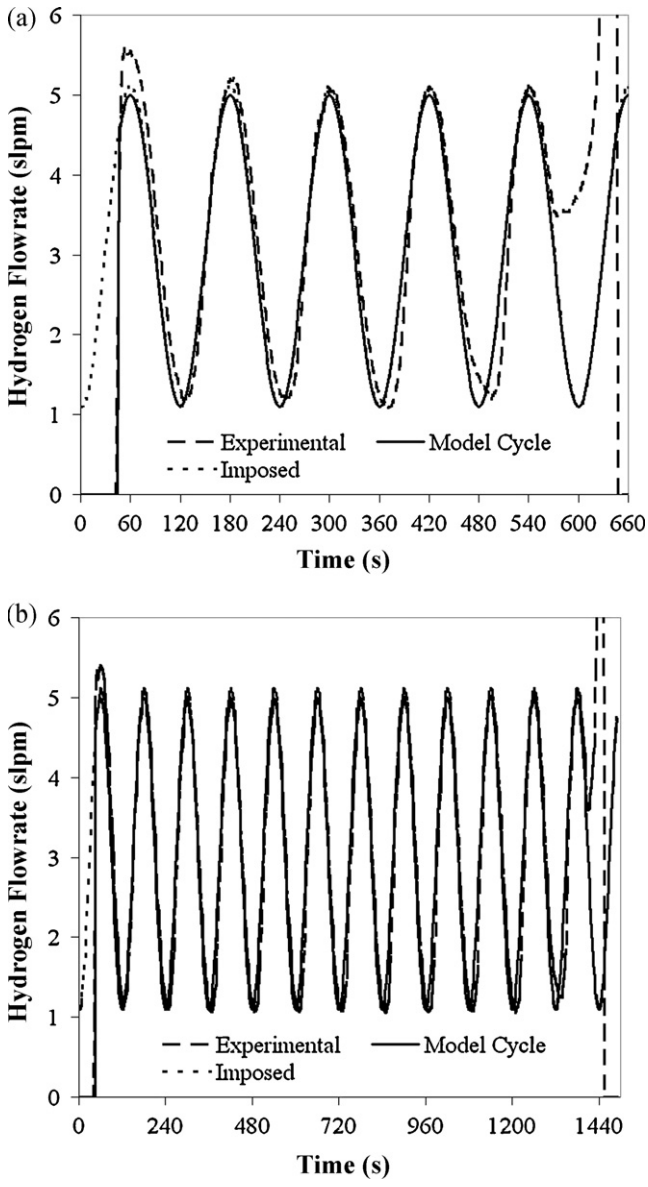

Fig. 9. Comparison of the flow rate of hydrogen exiting the tank showing the imposed flow rate as programmed in Labview, the flow rate recorded by the flow controller, and the theoretical flow rate that was generated for use in the model, (a) for the 25 °C scenario and (b) for the 35 °C scenario.

ment of parameters is investigated in Section 8 and the above noted compromise is described in further detail in Section 8.3.

8. Parametric analysis

A parametric study is performed to understand the differences between experimental and numerical results. For the dynamic scenario of this study these parameters are the shape of the PCT curve and the effective thermal conductivity. The base case of the model is as described in Section 6. For the parametric study only the 35 °C scenario is used. Results compare well with the 25 °C scenario, but there are an insufficient number of cycles to properly illustrate the effects.

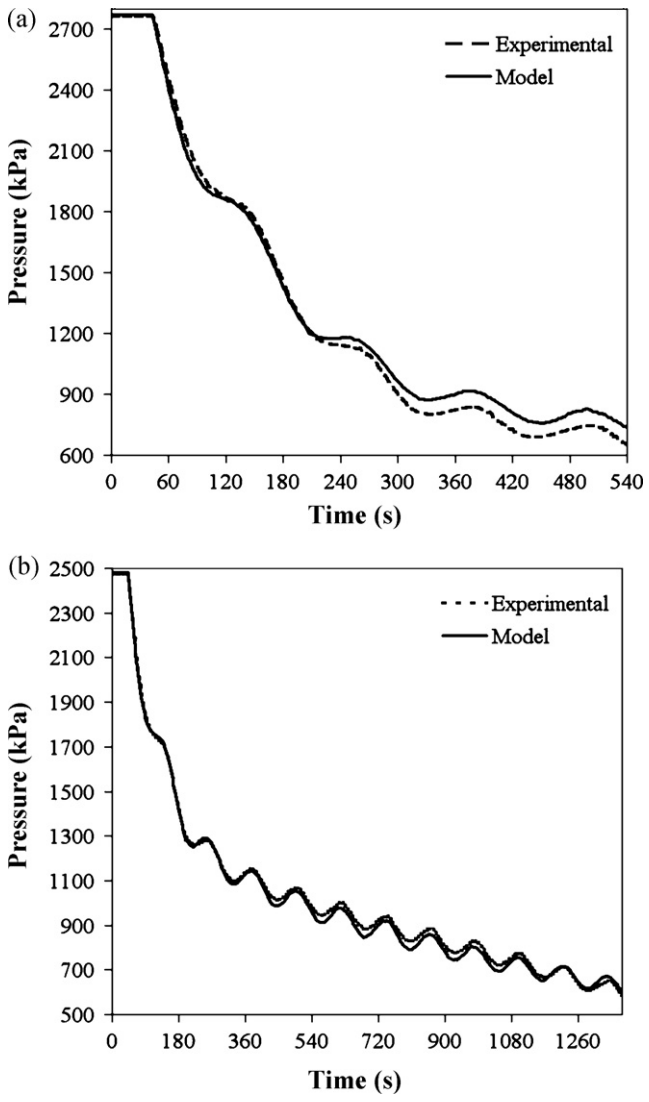

Fig. 10. Comparison of the metal hydride tank pressure yielded experimentally with the numerical model, (a) for the 25 °C scenario and (b) for the 35 °C scenario.

8.1. Tails for the PCT curve

The parametric analysis begins with a look at the tails that have been added to the equilibrium pressure isotherms. Much of the past modelling work has only dealt with the plateau pressure as described by the van't Hoff equation. It is important to compare the results of modelling with and without the tail regions included for a dynamic scenario to give future modellers an idea of the contribution of the tails and whether or not they will be important to their work. The comparison is therefore performed for a model with only the plateau region, the base model (includes the tails as described by Eqs. (6) and (7)), a model where the coefficient for the density term has been doubled for the upper tail region (base case coefficient is 0.0048 for P_{eqa} and 0.0059 for P_{eqd}), and a model where this coefficient has been halved. The reason for only altering the upper tail region is because the dynamic simulations describe desorption of a filled tank therefore the impact of the upper tail is more pronounced.

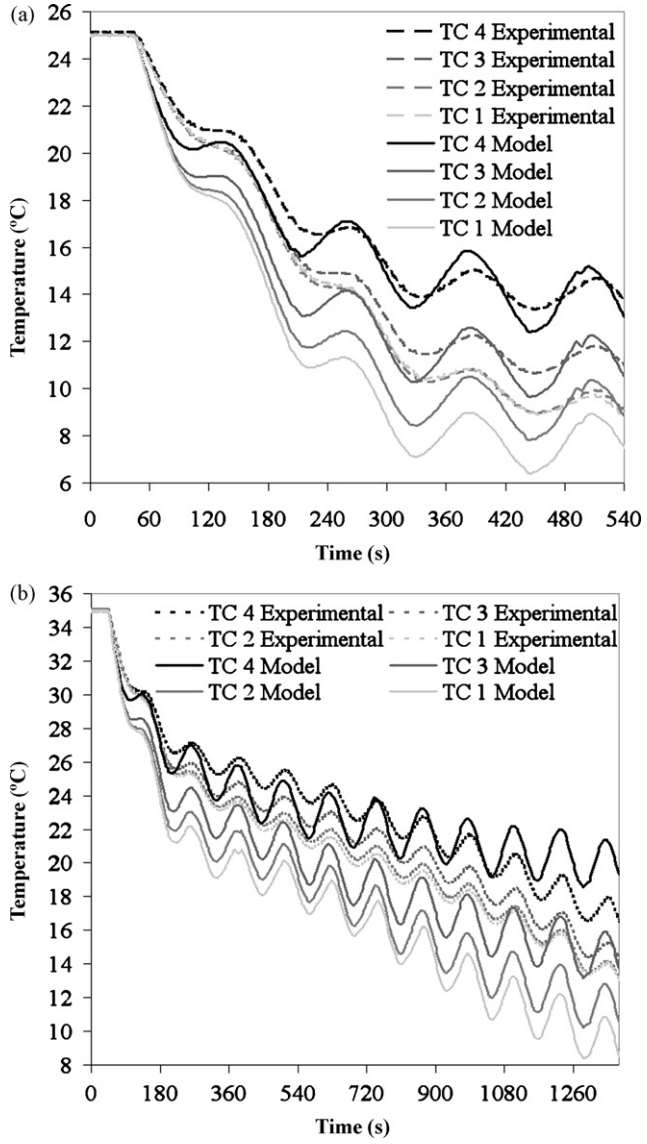

Fig. 11. Comparison of the temperature of the metal hydride bed at various radial distances yielded experimentally and predicted by the numerical model, (a) for the 25 °C scenario and (b) for the 35 °C scenario.

To simulate the four different cases, initial densities of the metal hydride bed must be determined. The initial pressure for modelling is the same as that recorded by the pressure transducer during the experiments. Since the tank has been brought to equilibrium at the temperature of the water bath, it can be assumed that the model should also start at an equilibrium point, which can be accomplished by selecting an initial density corresponding to the point on the PCT curve at the initial pressure of the experiments. This is not possible for the model where only the plateau region is described; therefore this case will begin at a density at the fullest extent of the plateau, which is 5580 kg m^{-3}. The base case begins at a density of 5589.3 kg m^{-3}, the doubled case begins at a density of 5586.6 kg m^{-3}, and the halved case begins at a density of 5593.2 kg m^{-3}. The results of these four models and the experimental data are shown in Fig. 12a for the pressure and Fig. 12b for the temperature comparison. Since there is minimal difference in the temperature plots, only the temperature at the most exterior thermocouple (TC 4 at 2.3 cm radius) has been plotted for comparison.

For the impact on the pressure inside the metal hydride tank it can be seen from Fig. 12a that altering the upper tail of the equilibrium pressure curve has the most impact during the first few cycles. When the density coefficient is doubled, the slope of the pressure curve is steeper. This equates to a sharper decline in the pressure of the tank as it empties during the first few cycles, an effect which seems to level off after a few cycles when the concentration of hydrogen in the alloy is mainly in the plateau region. The opposite effect is seen in Fig. 12a for the halved coefficient. Because the slope is flatter the decline in the pressure over the first few cycles is more gradual, the tank is better able to maintain a high pressure at the very beginning of its use cycle. The case where only the

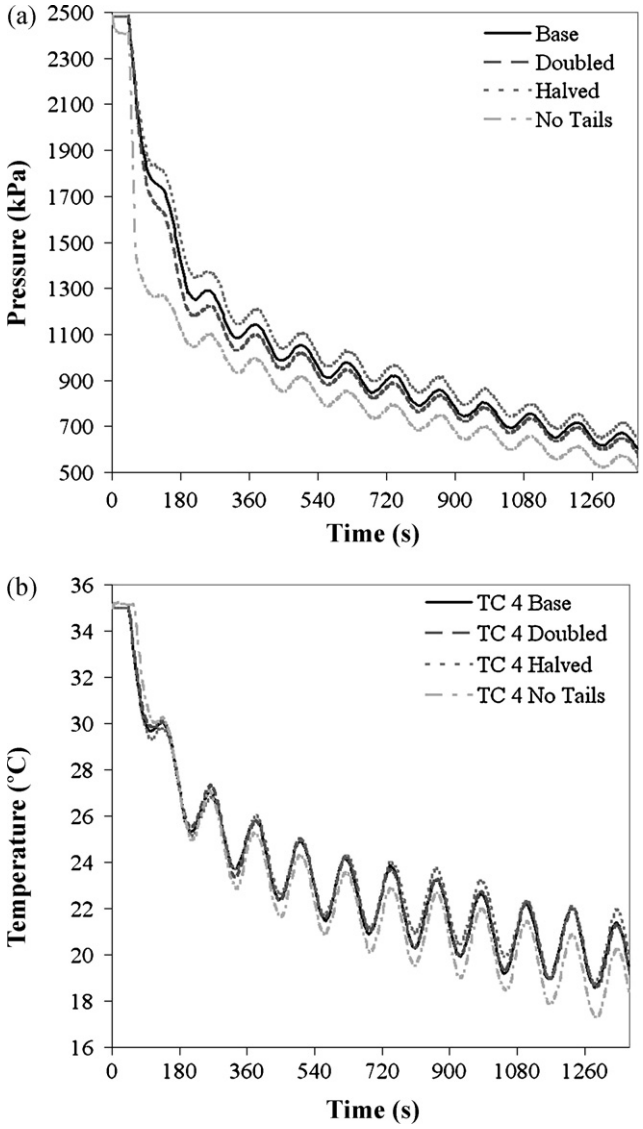

Fig. 12. (a) Comparison of the pressure predicted by the base model, a model with no tails, and two models with steeper and flatter tails, respectively for the 35 °C scenario. (b) Comparison of the temperature of the metal hydride bed at a radial distance of 2.286 cm predicted by the base model, a model with no tails, and two models with steeper and flatter tails, respectively for the 35 °C scenario.

plateau is modelled yields an initial decrease in pressure even before the tank begins cycling because the initial high pressure causes absorption to occur within the tank. Once the cycling begins there is a very steep drop in pressure as the tank empties until it reaches the level of the plateau at which point desorption begins to occur in the alloy and the pressure levels off somewhat. Since there is such a drastic drop in the pressure for the first few cycles, this model is less able to level off after a few cycles, and there is still a lower pressure being simulated even after 10 cycles, as compared to the base case. This demonstrates that the tails should be included in dynamic numerical modelling work when studying full or empty tanks where the pressure is an important result of the modelling work.

The impact of the tails on the temperature of the metal hydride bed is much less pronounced. It can be seen in Fig. 12b that there is very little appreciable difference in the temperature curves for each of the models. The lines are virtually overlapping each other. There is an initial anomaly for the plateau model due to the absorption described in the previous paragraph, but this corrects itself during the first cycle and the curve that follows is only slightly below the other models, resulting from the lower pressure experienced. This indicates that for dynamic modelling work where temperatures are the key result, inclusion of the equilibrium pressure tail regions is not as important as it is for pressure behaviour.

8.2. Slope of the PCT plateau region

The concentration dependence of the equilibrium pressure is examined by changing the coefficient of the density term (base coefficient is 0.01116 in Eqs. (6) and (7)) which can also be described as changing the slope of the plateau region. The comparison is performed for a model with a flat plateau slope (about the centre point of the base case plateau), the base case, and a model with a doubled slope (about the centre point of the plateau, on a logarithmic scale).

Altering the slope of the plateau region also adjusts the starting point for the upper tail, as illustrated in Eqs. (6) and (7). This means that the initial densities must be determined for each case in the same manner as they were calculated in Section 8.1. The base case begins at a density of 5589.3 kg m^{-3}, the flat plateau case begins at a density of 5592.5 kg m^{-3}, and the doubled case begins at a density of 5584.4 kg m^{-3}. The results of these three models are shown in Fig. 13 for the pressure, and Fig. 14a and b for the temperature comparison.

In regards to the impact of the slope of the plateau region on the pressure within a metal hydride tank, Fig. 13 shows that it is significant. The model with a flat plateau slope yields a significantly lower pressure than the base model at the beginning of cycling, which is due to the lower equilibrium pressure at a higher state of fill. Although it appears to equalize with the base model, it is not believed this would continue for further cycling. It is expected that if the tank was to empty more the pressure would cross the base curve and yield higher pressures, since at a lower state of fill there would be a higher equilibrium pressure. The doubled plateau slope shows the same effect as

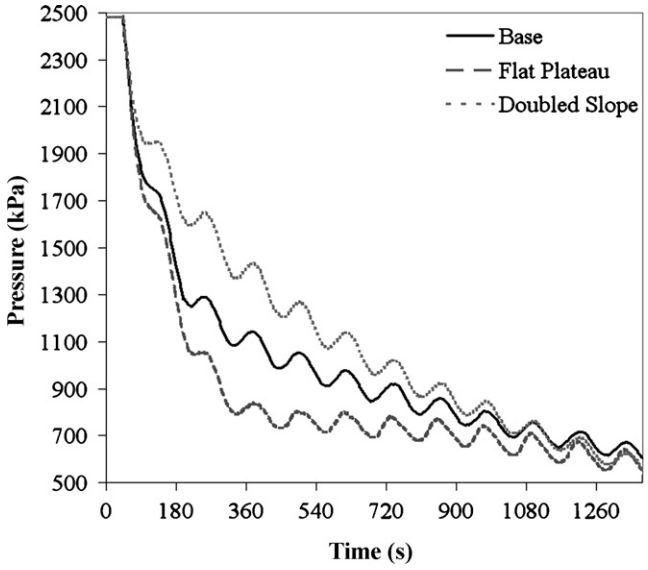

Fig. 13. Comparison of the pressure predicted by the base model, a model a flat plateau region, and a model with a doubled plateau slope for the 35 °C scenario.

the flat slope but in reverse, since the equilibrium pressures are higher at a higher state of fill and lower when the state of fill is lower. This illustrates that concentration dependence for the plateau region of equilibrium pressure curves is an important parameter to include in dynamic modelling scenarios for the alloy being investigated if accurate pressures are required. This result emphasizes the importance of determining the nature of the slope of the equilibrium pressure plateau for alloys involved in future modelling work and including it in the models to ensure accurate pressure behaviour is obtained.

With respect to the impact of concentration dependence of the plateau region on the radial temperature profile of metal hydride beds, Fig. 14a and b shows that it is significant. The model with a flat plateau slope yields rising peak temperatures over the 480–840 s range, and a reduced spread of temperature across the radial direction as the tank empties. This behaviour is due to a more concentrated reaction zone for a model with a flat plateau slope. A model with a concentration slope will yield a more spread out reaction zone because higher equilibrium pressures associated with more full metal hydride alloy make desorption more likely to occur in alloy that is more full. Since the tank starts out as being full the reaction will occur over more of the bed, even though heat may not be penetrating the more central regions. This causes a more spread out reaction as opposed to a more concentrated wave-like reaction that the authors describe in previous papers [17,18] for a flat plateau slope. The model with a doubled plateau slope does not yield the same type of rising or decreasing effect as seen with the flat slope, but it yields radial temperatures that are more spread out over the metal hydride bed as the tank empties for the reasons described above. The temperature plots further emphasize the importance of determining the nature of the plateau slope for the alloy being used in modelling work, since the temperature behaviour can vary significantly for different slopes.

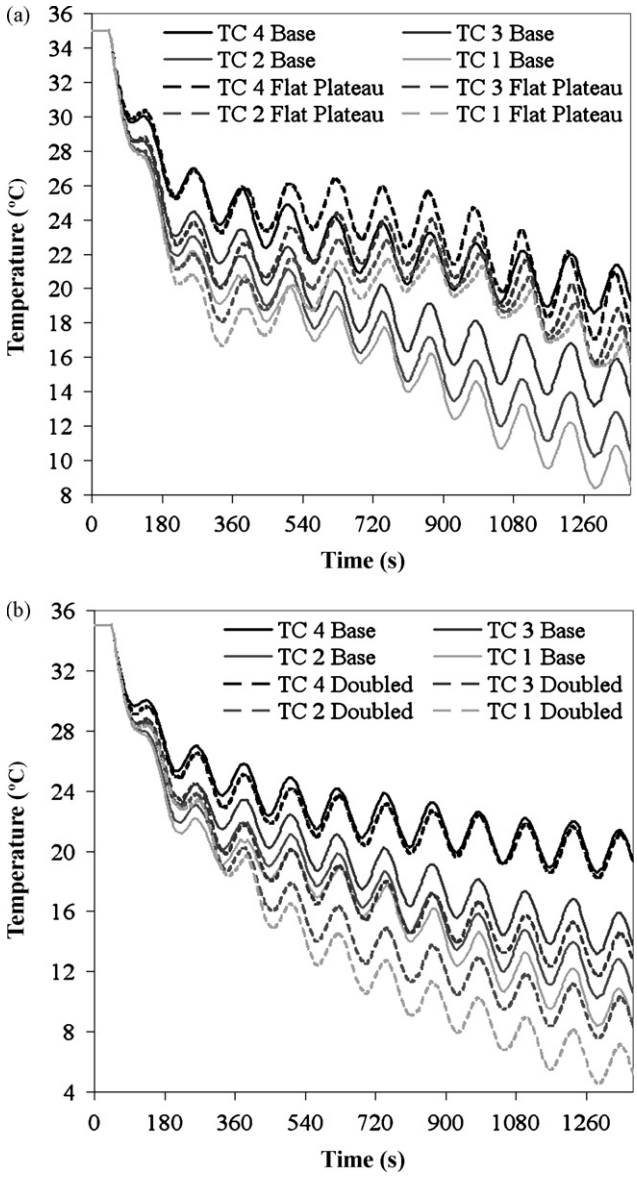

Fig. 14. (a) Comparison of the temperature of the metal hydride bed at various radial distances generated with the base model, and a model a flat plateau region for the 35 °C scenario. (b) Comparison of the temperature of the metal hydride bed at various radial distances generated with the base model, and a model with a doubled plateau slope for the 35 °C scenario.

8.3. Effective thermal conductivity

The thermal conductivity is a parameter where the authors have assumed a constant value in previous studies [17,18], but due to varying opinions in the literature would like to quantify the impact for dynamic scenarios. The base model in this study uses an expression for thermal conductivity that contains both concentration and pressure dependence as described in Section 5. A comparison is performed for the base case, two models with different constant values for thermal conductivity (the first is estimated based on the average thermal conductivity of the bed in a base case simulation (2.2 W m K^{-1}), and a second case where this value is doubled), and a model where the effective thermal conductivity as described in Eq. (9) is doubled, thus

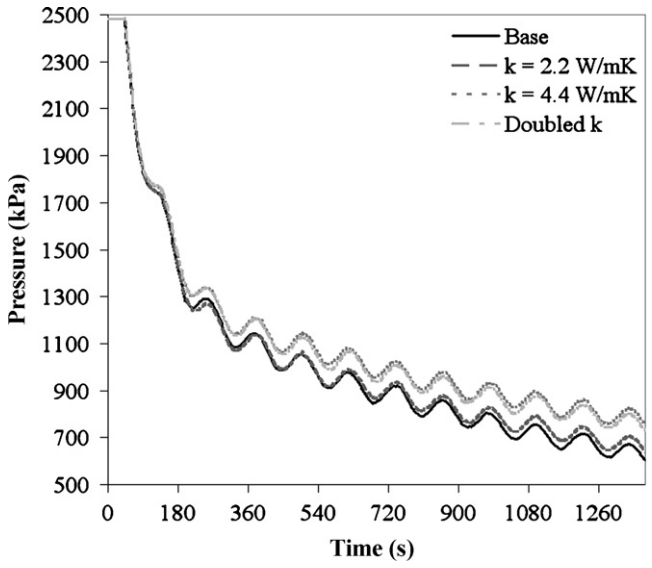

Fig. 15. (a) Comparison of the pressure predicted by the base model, two models with an averaged and doubled constant effective thermal conductivity values, respectively, and a model with a doubled effective thermal conductivity expression for the 35 °C scenario.

doubling the conductivity of the bed while at the same time effectively doubling the effect of the concentration and pressure dependence. The results of these four models and the experimental data are shown in Fig. 15 for the pressure, and Fig. 16a–c for the temperature comparison.

It can be seen from Fig. 15 that altering thermal conductivity has an impact on the resulting pressure behaviour from the model that is somewhat minor. The case with an average constant value yields a slightly lower pressure when the tank has a higher state of fill and higher pressure as the tank empties. This is to be expected since the base case has higher thermal conductivities for higher pressures and concentrations and lower thermal conductivity for lower pressures and concentrations, while the constant case merely lies in the middle of these extremes. Fig. 15 also shows that higher thermal conductivities yield higher pressure, which is also to be expected, since there is more heat transfer and therefore the metal hydride tank can release more hydrogen and maintain a higher pressure.

When examining the impact of thermal conductivity on the temperature profiles Fig. 16a–c shows that there is a significant change in the radial temperature profile of the metal hydride bed. For the constant average thermal conductivity the effect was similar to the pressure behaviour described in the previous paragraph for the same reasons (lower temperatures in early cycling and higher temperatures as the tank empties). Also similar to the pressure behaviour, the higher thermal conductivities yield higher temperatures but the overall significance is more pronounced when compared to the pressure change. Also of note is that the higher thermal conductivities maintain a more steady temperature across the radius of the tank, as can be seen from the curves for the different radii being closer together near the end of cycling. It can be seen in Fig. 11a and b, that although the base case model presented in this study agrees well with the experimental data, it is not a perfect fit. The experimental curves

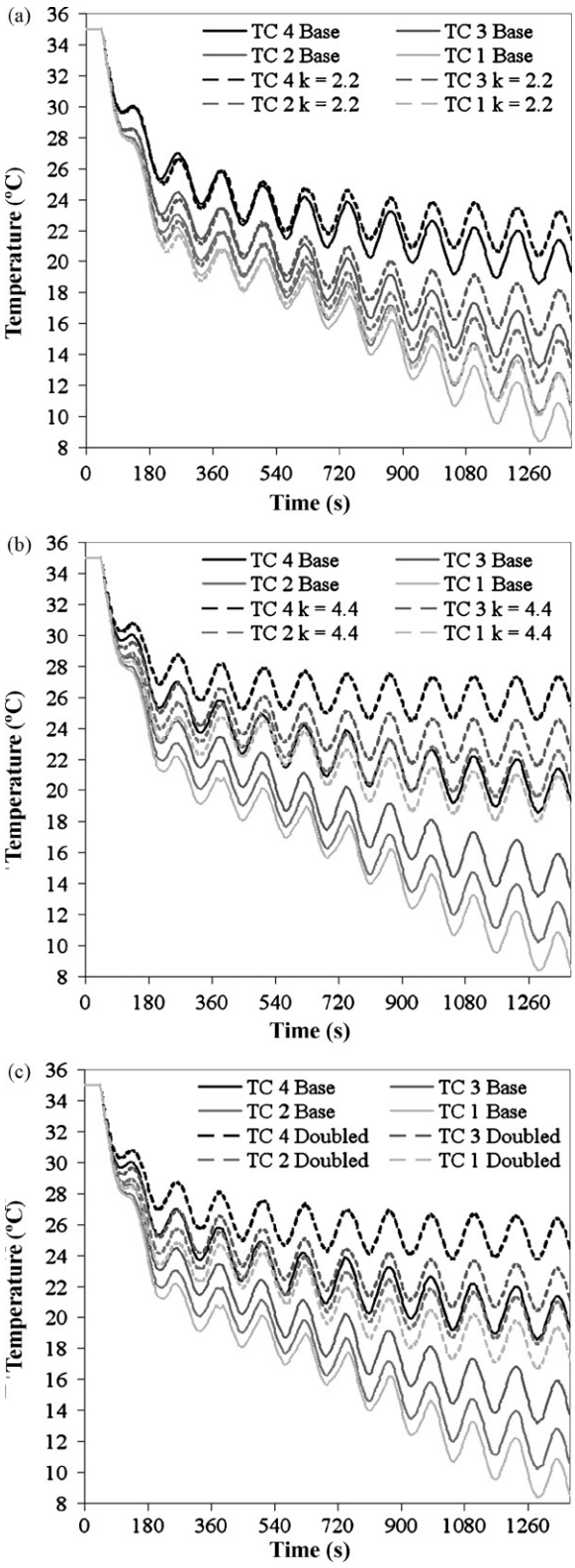

Fig. 16. (a) Comparison of the temperature of the metal hydride bed at various radial distances generated with the base model, and a model with an averaged constant effective thermal conductivity value for the 35 °C scenario. (b) Comparison of the temperature of the metal hydride bed at various radial distances generated with the base model, and a model with a doubled constant effective thermal conductivity value for the 35 °C scenario. (c) Comparison of the temperature of the metal hydride bed at various radial distances generated with the base model, and a model with a doubled effective thermal conductivity expression for the 35 °C scenario.

maintain a more steady temperature across the radius of the tank as compared to the modelling results. This could be corrected by increasing the thermal conductivity, but the pressure behaviour and also the overall decay in the temperatures as the tank empties would suffer. Therefore it can be seen from the analysis in this section that the base model is a compromise between these factors. This section also shows that utilization of an effective thermal conductivity relationship that includes pressure and concentration dependence can be important in modelling work and generate more accurate results.

9. Conclusions

Dynamic metal hydride storage systems were analyzed by a combination of experimental tests and numerical modelling simulations. The experimental results enabled the validation of a numerical model developed and utilized by the authors in previous studies [17,18] and further improved in this study for simulating dynamic applications. The authors were also able to perform a parametric analysis on some of the important variables in metal hydride modelling in order to improve the understanding of how these parameters affect modelling results and make it easier for future numerical models to be developed and used. Including tails on the equilibrium pressure curves was found to be important particularly for the accuracy of the initial cycles. Introducing a concentration dependence for the plateau region of the equilibrium pressure curve was found to be important for both pressure and temperature results and it would be advisable to investigate the slope of the plateau for the metal hydride alloy that is modelled. Effective thermal conductivity was found to be important, and the inclusion of pressure and concentration dependence produced more precise modelling results.

Acknowledgements

This work was supported by the AUTO21 research initiative and the Natural Sciences and Engineering Research Council of Canada.

References

[1] G. Sandrock, J. Alloys Compd. 293–295 (1999) 877–888.
[2] U. Mayer, M. Groll, W. Supper, J. Less-Common Met. 131 (1987) 235–244.
[3] D. Sun, S. Deng, J. Less-Common Met. 141 (1988) 37–43.
[4] D. Sun, S. Deng, J. Less-Common Met. 155 (1989) 217–279.
[5] D. Sun, S. Deng, Int. J. Hydrogen Energy 15 (1990) 807–816.
[6] M.R. Gopal, S.S. Murthy, Int. J. Hydrogen Energy 17 (1992) 795–805.
[7] M.R. Gopal, S.S. Murthy, Chem. Eng. Proc. 32 (1993) 217–223.
[8] A. Jemni, S. Ben Nasrallah, Int. J. Hydrogen Energy 20 (1995) 43–52.
[9] A. Jemni, S. Ben Nasrallah, Int. J. Hydrogen Energy 20 (1995) 881–891.
[10] S. Ben Nasrallah, A. Jemni, Int. J. Hydrogen Energy 22 (1997) 67–76.
[11] A. Jemni, S. Ben Nasrallah, J. Lamloumi, Int. J. Hydrogen Energy 24 (1999) 631–644.
[12] F. Askri, A. Jemni, S. Ben Nasrallah, Int. J. Hydrogen Energy 28 (2003) 537–557.
[13] F. Askri, A. Jemni, S. Ben Nasrallah, Int. J. Hydrogen Energy 29 (2004) 635–647.
[14] M. Mat, Y. Kaplan, Int. J. Hydrogen Energy 26 (2001) 957–963.
[15] A. Demircan, M. Demiralp, Y. Kaplan, M.D. Mat, T.N. Veziroglu, Int. J. Hydrogen Energy 30 (2005) 1437–1446.

[16] T. Nakagawa, A. Inomata, H. Aoki, T. Miura, Int. J. Hydrogen Energy 25 (2000) 339–350.
[17] B. MacDonald, A. Rowe, Int. J. Hydrogen Energy 31 (2006) 1721–1731.
[18] B. MacDonald, A. Rowe, J. Power Sources 161 (2006) 346–355.
[19] E.S. Kikkinides, M.C. Georgiadis, A.K. Stubos, Int. J. Hydrogen Energy 31 (2006) 737–751.
[20] E.S. Kikkinides, M.C. Georgiadis, A.K. Stubos, Energy 31 (2006) 2428–2446.
[21] S. Suda, N. Kobayashi, K. Yoshida, Y. Ishido, S. Ono, J. Less-Common Met. 74 (1980) 127–136.
[22] S. Suda, N. Kobayashi, K. Yoshida, Int. J. Hydrogen Energy 6 (1981) 521–528.
[23] E. Suissa, I. Jacob, Z. Hadari, J. Less-Common Met. 104 (1984) 287–295.
[24] A. Kempf, W.R.B. Martin, Int. J. Hydrogen Energy 11 (1986) 107–116.
[25] D. Sun, S. Deng, J. Less-Common Met. 160 (1990) 387–395.
[26] M. Pons, P. Dantzer, Int. J. Hydrogen Energy 19 (1994) 611–616.
[27] E. Hahne, J. Kallweit, Int. J. Hydrogen Energy 23 (1998) 107–114.
[28] D. Sun, S. Deng, Int. J. Hydrogen Energy 15 (1990) 331–336.
[29] M. Pons, P. Dantzer, J. Less-Common Met. 172–174 (1991) 1147–1156.
[30] Z. Jiang, R.A. Dougal, S. Liu, S.A. Gadre, A.D. Ebner, J.A. Ritter, J. Power Sources 142 (2005) 92–102.
[31] O. Bernauer, J. Topler, D. Noreus, R. Hempelmann, D. Richter, Int. J. Hydrogen Energy 14 (1989) 187–200.
[32] F.P. Incropera, D.P. DeWitt, Fundamentals of Heat and Mass Transfer, 5th ed., John Wiley and Sons, New York, 2002.